aerospace

MDPI

Article

Effect and Mechanism of Roughness on the Performance of a Five-Stage Axial Flow Compressor

Yan Chen [1,2,*], Chunxiang Gao [1] and Wuli Chu [1,2]

[1] School of Power and Energy, Northwestern Polytechnical University, Xi'an 710129, China
[2] Shaanxi Key Laboratory of Thermal Science in Aero-Engine System, Northwestern Polytechnical University, Xi'an 710072, China
* Correspondence: xjtu.chenyan@nwpu.edu.cn; Tel.: +86-136-4927-6660

Abstract: In order to prolong the service life of multistage axial compressors, it is increasingly important to study the influence of blade surface roughness on the compressor performance. In this paper, a five-stage axial compressor of a real aero-engine was selected as the research object, and an equivalent gravel roughness model was used to model the roughness based on measured blade surface roughness data. Furthermore, the impact of blade surface roughness on the performance at design rotational speed was studied by full three-dimensional numerical simulation, and the mechanism of performance variation caused by the roughness was discussed combined with quantitative and flow field analyses. The results show that, when the blade surface roughness of all blades increases, the peak total efficiency decreases by approximately 0.4%, the blocking mass-flow decreases by approximately 0.3%, and the stable working range changes little. When the surface roughness of all rotor blades increases, the performance decline is close to that of all rotor and stator blades, and the variation in stator blade roughness has little effect on the compressor performance. Regarding the variation in roughness, the performance of the latter stage is more sensitive than that of the previous stage, and the decline in the performance of the fifth stage contributes the most to the total performance degradation of the compressor. Once the surface roughness of the fifth-stage rotor blade increases, the flow in the middle of the rotor blade deteriorates and the stage performance decreases obviously, which is the main reason for the decline in the overall performance.

Keywords: multistage axial compressor; equivalent gravel roughness; quantitative analysis; full three-dimensional numerical simulation

Citation: Chen, Y.; Gao, C.; Chu, W. Effect and Mechanism of Roughness on the Performance of a Five-Stage Axial Flow Compressor. *Aerospace* **2022**, *9*, 428. https://doi.org/10.3390/aerospace9080428

Academic Editor: Sebastian Karl

Received: 14 June 2022
Accepted: 29 July 2022
Published: 4 August 2022

1. Introduction

Aeroengines generally work under extremely harsh conditions, such as a high temperature, high pressure, high speed, and high load. Working in extreme environments (i.e., humidity, offshore low altitude, and heat) for a long time, many particles and pollutants inhaled by the engine will continuously impact, wear, and corrode the engine blades or accumulate dirt on the blade surface [1], which causes changes in blade surface roughness. Hence, the performance of the whole engine becomes worse: the working efficiency is reduced and the fuel consumption rate is increased, which have attracted people's attention to the study of blade surface roughness. As one of the three major components of aeroengines, the compressor is a vital part. By studying the influence of blade surface roughness on the compressor performance, it is helpful to monitor the surface roughness of aeroengines in actual operations, thereby formulating a reasonable maintenance interval and maintenance procedure, as well as prolonging the service life.

There is much literature concerning roughness fluid mechanics and wall turbulence [2–8]. For example, Yuan et al. [2] carried out direct numerical simulation in open-channel flows over sand grain roughness in transitionally and fully rough regimes. The results showed that, in the fully rough regime, roughness directly affects the generation

of the wall-normal fluctuations, whereas, in the transitionally rough regime, the region affected by roughness is separated from the region of the intense generation of these fluctuations. Yang et al. [3] conducted a series of large eddy simulations of turbulent boundary layers over arrays of cuboidal roughness elements at arbitrary orientation angles. The results suggested the necessity of accounting for detailed rough wall topology when relating rough wall morphology to its aerodynamic properties. Redford et al. [8] used direct numerical simulation to study the transition to turbulence of a high-speed boundary layer over a flat plate with an isolated roughness element. It was found that acoustic disturbances were more efficient at stimulating the shear layer instability compared with upstream boundary layer disturbances, perhaps because the boundary layer near the roughness element is particularly receptive to external disturbances. The above literature shows that roughness has a great influence on wall flow, so it is of practical engineering significance to study the influence of blade roughness on the compressor performance.

The research of compressor blade roughness is a research hotspot of scholars globally. Bammert et al. [9] employed a low-speed compressor cascade as the research object and found that the increase in roughness led to the separation of the boundary layer near the trailing edge of the suction surface. Back et al. [10] concluded that the deviation angle and the loss of a cascade increase with the increase in roughness by using experimental methods on the overall roughness of the blade surface. Suder et al. [11] combined experimental data with numerical simulation to study the effect of roughness change on the performance of a transonic compressor, NASA Rotor 37. The results show that the increment of roughness reduced the compressor efficiency and pressure ratio at the design condition by 6% and 9%, respectively. Morini et al. [12–14] conducted many numerical simulation studies related to compressor blade roughness, indirectly verified the reliability of the numerical simulation, and analyzed the impact of blade surface roughness on the performance of a compressor stage, NASA stage 37. Finally, it was found that the blade surface roughness had little effect on the efficiency of the blockage region, and the rotor surface roughness had a greater impact on the compressor performance.

Although the research on compressor blade roughness in China has been carried out late, many studies have also been carried out. Gao et al. [15] pasted sandpaper on the surface of a compressor cascade and then studied the aerodynamic characteristics of the cascade with sandpaper through experiments, which demonstrated that the influence of blade surface roughness on aerodynamic losses cannot be ignored. Liu et al. [16] studied the impact of blade roughness on a low-speed compressor cascade; it was found that, with an increase in roughness, the total pressure loss increases and the corner separation phenomenon intensifies. Wang et al. [17] numerically simulated the effects of roughness on the performance of a high-subsonic compressor cascade, showing that, when the Reynolds number was reduced to 1.5×10^5, excessive roughness would cause the deterioration of the cascade performance. Moreover, using the numerical simulation of a single-stage compressor, Chen et al. [18] revealed that, as the roughness increases, the impact of roughness on the performance of the rotor and the whole stage was almost the same, whereas the impact on the performance of the stator was relatively small.

In the published literature, the research objects for investigating the impact of compressor roughness are limited to a cascade, single rotor, and single-stage compressor, while there is relatively little research on the roughness of multistage axial compressors. Whether the conclusions of the influence of blade roughness on the performance of a single rotor or single-stage compressor apply to a multi-stage compressor is worthy of an in-depth study. In addition, the number of studies on using the real size of blade roughness is limited. In the current studies, the roughness is mostly given by a hypothesis, and there may be a certain difference between the given roughness and the roughness in the real situation, which also leads to the difference between the impact of blade roughness on the compressor performance and the actual impact. Therefore, the real measurement data of compressor blade surface roughness-based research are more meaningful for engineering practice. Furthermore, in order to address how the roughness effect can be mitigated by

optimal design control, much literature [19–24] provides design methods and optimization approvals. In particular, literature [22] provides a detailed optimization design method for turbomachinery, which provides an effective means for the performance improvement of turbomachinery. However, the amount of CFDs for the optimal design of all blades of multistage compressors is huge. To alleviate the calculation burden, it is important to develop a method before optimization to determine which compressor stage roughness change has the greatest impact on the overall performance.

In the present study, the equivalent gravel roughness model was employed to model the blade surface roughness based on actual measured blade surface roughness data. Then, a five-stage axial low-pressure compressor of an engine in service was chosen as the research object, and the full three-dimensional numerical simulation method was utilized to study the influence of the change in blade surface roughness on the aerodynamic performance at the design rotational speed. In addition, a quantitative analysis method was used to determine the compressor stage whose roughness change has the greatest impact on its performance. Finally, by analyzing the details of the flow field, the mechanism for the influence of blade roughness of the compressor stage on the whole compressor was further explored.

2. Description of Research Methods

2.1. Research Object

The research object of this paper was a five-stage axial low-pressure compressor in service, as shown in Figure 1. The numerical calculation model of the low-pressure compressor included an inlet rectifier cone, inlet guide vane (IGV), rotor blades (R*i*), and stator blades (S*i*), in which, R1 and R5 were equipped with blade dampers. At the design rotational speed, the flow coefficient was 0.66, and the inlet Mach number of R1 was 1.20. Some design parameters of the compressor at the design rotational speed are shown in Table 1.

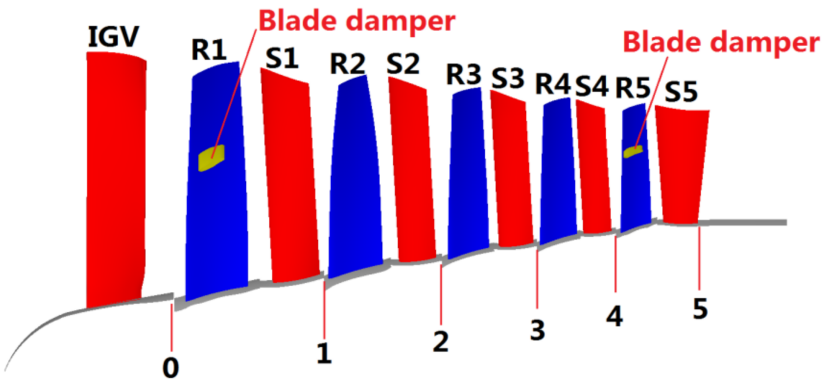

Figure 1. Structural diagram of multistage compressor.

Table 1. Some design parameters of multistage compressor.

Parameter	Value
Design rotational speed	7952 r/min
Total pressure ratio	2.95
Pressure ratio of 1st stage	1.29
Pressure ratio of 2nd stage	1.30
Pressure ratio of 3rd stage	1.21
Pressure ratio of 4th stage	1.22
Pressure ratio of 5th stage	1.20

2.2. Validations of Numerical Schemes

The mesh with a single passage for numerical calculations was generated by NUMECA/Autogrid5. An O4H topology was used for each blade row, and a butterfly grid was applied for the rotor tip clearance. Since there is a damper in the position of R1 and R5 in the blade, the grid around the damper was densified, as shown in Figure 2. The verification of the computational grid independence is shown in Figure 3. The total number of grids for the five-stage compressor reached 5 million, which was verified by grid independence. When the number of grids increases to 7 million and 9 million, its performance curves (mass flow rate to pressure ratio) are almost consistent with those of 5 million grids. Therefore, the number of 5 million grids was selected for numerical simulations. All grids were densified near the wall, and the first grid distance was 0.005 mm to ensure $Y^+ < 5$. Figure 4 gives the Y^+ distributions for all blade walls. It can be seen that the maximum Y^+ is less than 5, which is enough to meet the calculation requirement.

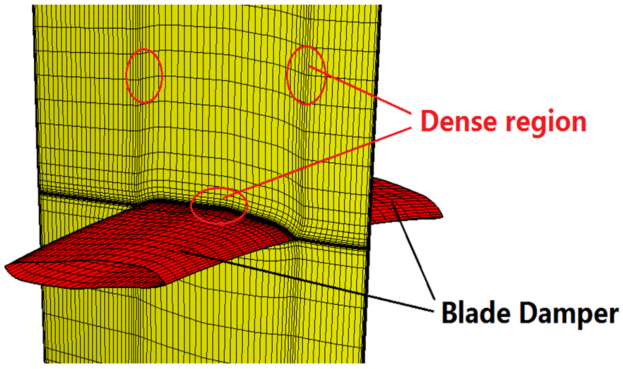

Figure 2. Schematic diagram of grid details for R1 and R5.

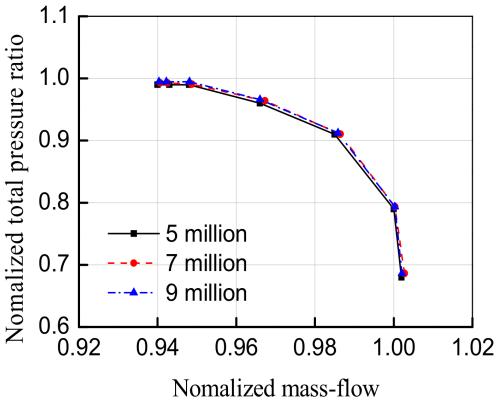

Figure 3. The verification of the computational grid independence.

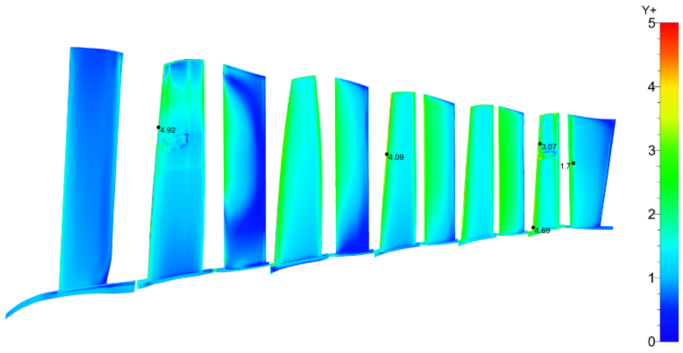

Figure 4. Y^+ distributions for all blade walls.

Commercial software NUMECA/FineTurbo was employed for numerical calculations of the mesh at the design rotational speed. Assuming that the working medium is an ideal gas, the three-dimensional Reynolds-averaged Navier–Stokes (N–S) equation in the relative coordinate system is solved by the central difference scheme in finite volume method. Because the roughness has small-scale geometric change, the enhanced wall equation needs to be used to capture the near-wall flow changes caused by roughness. Therefore, the Spalart–Allmaras (S–A) turbulence model with enhanced wall function was selected to close the N–S equation. In the calculation process, the explicit fourth-order Runge–Kuta method was used for time discretization, and the second-order upwind scheme based on flux difference discrete scheme was applied for spatial discretization. The total pressure, total temperature, and axial inflow angle were given at the inlet boundary, and the average static pressure was imposed at the outlet. In addition, all solid walls were defined as adiabatic non-slip boundary conditions. Furthermore, the mixing plane was used at the rotor–stator interface to ensure the accurate transmission of flow, momentum, and energy information between rotors and stators.

To verify the accuracy of the above numerical schemes, the total performance of the compressor obtained by experimental measurement and numerical simulation at the design rotational speed is compared in Figure 5. In Figure 5, the total pressure ratio and the mass flow are normalized values, which are, respectively, compared with the experimentally measured peak pressure ratio and blocking mass flow. It is shown that the numerical values are in good agreement with the experimental values, indicating that the numerical schemes can be used to carry out relevant research. Moreover, there is a certain error between the experimental data and the numerical simulation results, which may be due to the heat transfer on the wall of the hub during the experiment and the adiabatic setting during the numerical simulation.

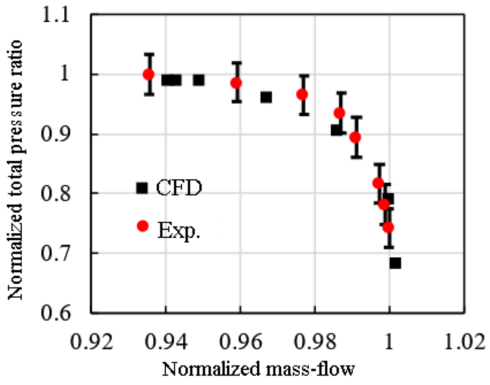

(**a**)

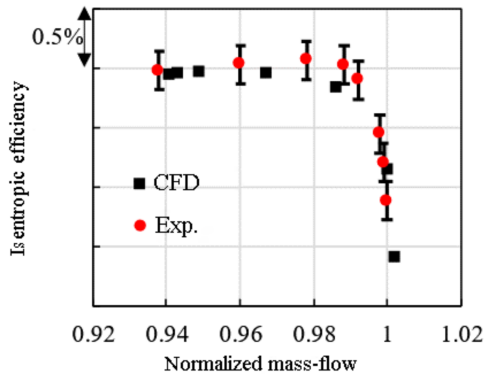

(**b**)

Figure 5. Comparison of overall performance at design rotational speed between experimental measurement and numerical simulation. (**a**) Total pressure ratio versus mass flow, (**b**) Isentropic efficiency versus mass flow.

2.3. Equivalent Gravel Roughness Model

The evaluation parameters of surface roughness include amplitude parameters, spacing parameters, and shape characteristic parameters. The amplitude parameters represent the evaluation parameters of the height direction of surface roughness. The spacing parameters and shape characteristic parameters describe the evaluation parameters of the horizontal direction of surface roughness. The roughness measured in engineering generally refers to the arithmetic mean deviation R_a of the contour in the amplitude parameter, which is defined as the arithmetic mean of the absolute value of the surface micro contour offset $Z(X)$ within the sampling length l_r. The specific expression is as follows:

$$R_a = \frac{1}{l_r}\int_0^{l_r} |Z(X)|dX \tag{1}$$

However, since the evaluation parameters of surface roughness are not determined by amplitude parameters, the roughness R_a defined in engineering cannot fully characterize the surface roughness. Schlichting [25] first proposed the equivalent gravel roughness K_s to characterize the surface roughness. Under the condition of uniform flow, the actual rough surface is equivalent to a surface covered by a layer of uniform spherical gravel with a diameter of K_s. The definition diagram of equivalent gravel roughness is shown in Figure 6.

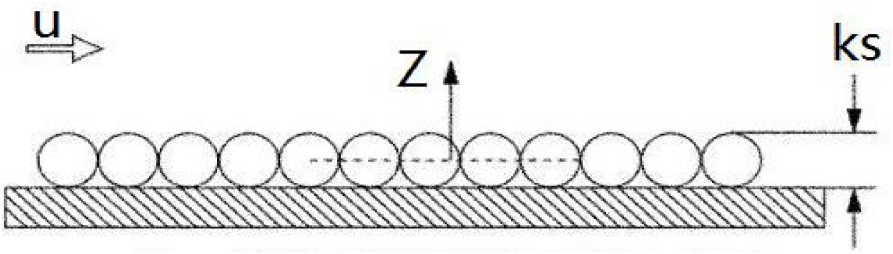

Figure 6. Schematic diagram of equivalent gravel roughness.

Compared with the traditional roughness evaluation parameter R_a, the equivalent gravel roughness K_s considers the amplitude, shape, and density of the actual rough surface micro contour at the same time, which is widely used in the study of surface roughness [26]. In order to determine the relationship between K_s and R_a, Bons [27] counted the conversion relationship between different roughness evaluation parameters by many scholars. For the engine blade surface, K_s is generally greater than $5R_a$ and less than $10R_a$. In the present work, the research on roughness adopted the hypothesis of Koch and Smith [28], that is, taking $K_s = 6.2R_a$.

To simulate the effect of blade surface equivalent gravel roughness on the performance of the multistage compressor, it is necessary to modify the enhanced wall function under the condition of a smooth wall. For the S–A turbulence model in NUMECA/FineTurbo, the enhanced wall function under rough wall conditions needs to be modified as:

$$\frac{u}{u_\tau} = \frac{1}{k}\ln(\frac{y}{v}u_\tau) + B_0 - \Delta U^+ \tag{2}$$

where u is the near-wall velocity; u_τ is the friction speed; Carmen constant k is 0.41; y is the first layer height of grids near the wall; v is the dynamic viscosity coefficient of the fluid; ΔU^+ is a function related to Reynolds roughness $K_s{}^+ = (u_\tau \cdot K_s)/v$. For completely rough wall surfaces such as compressor blades, the functional relationship is as follows:

$$\Delta U^+ = \frac{1}{k}\ln k_s^+ + B_0 - 8.5 + e^{(a_1 k_s^+ + a_2)} \tag{3}$$

where constants $a_1 = -0.7649$, $a_2 = 1.9$. After substituting Equation (3) into Equation (2), the enhanced wall function can be expressed as

$$\frac{u}{u_\tau} = \frac{1}{k}\ln\left(\frac{yu_\tau}{vk_s^+}\right) - e^{(a_1 k_s^+ + a_2)} + 8.5 \quad (4)$$

Equation (4) is a new method to calculate the enhanced wall function, which indicates that the enhanced wall function is independent of parameter B_0. It should be noted that this new calculation method requires the first layer height of grids $y \geq 1/2\ K_s$.

3. Results and Discussion

In the actual multistage axial compressor, the distribution of roughness on the blade surface is uneven. However, considering the huge workload of numerical simulations for the five-stage compressor, this paper assumes that the roughness distribution on the suction surface and pressure surface of each blade is uniform. After field investigation in the factory, the traditional roughness evaluation parameter R_a of the five-stage compressor blade was measured and averaged. Finally, according to $K_s = 6.2R_a$, the equivalent gravel roughness value of each blade suction and pressure surface was obtained, as shown in Table 2. From Table 2, it is seen that the roughness of R1 and R5 is inconsistent with that of other rotors. This is because the blade material for R1 and R5 is inconsistent with that of other blades.

Table 2. Equivalent gravel roughness of suction and pressure surfaces at all stages.

	Suction Surface μm	**Pressure Surface μm**
R1	14.35	10.39
R5	8.75	7.59
Rest rotors	10.45	8.49
All stators	9.37	7.26

In this section, when studying the influence of blade surface roughness on the performance of the compressor at the design rotational speed and deeply excavating the mechanism of the influence, the roughness involved adopts the real data obtained in Table 2.

3.1. Influence of Roughness Variation on Compressor Overall Performance

Figure 7 presents the overall performance curves of the compressor at the design speed with the variation in blade surface roughness. The three curves from top to bottom represent the total performance curves of all blades polished (ABP), all blades roughened (ABR), and all rotors roughened individually (ARRI), respectively. It is observed that, when all blades become rough, the blocking flow, peak total pressure ratio, and peak total efficiency are reduced. Compared with the situation of all blades polished, the blocking mass flow decreases by approximately 0.3%, and the peak total efficiency decreases by approximately 0.4%. However, the stable working range changes little, which is consistent with the conclusion of Chen et al. [19] in the roughness study for NASA stage 35. Therefore, the blade roughness has little effect on the stable working margin of the compressor. When all of the rotor blades become rough, the compressor performance curve is close to the case with all rough blades, demonstrating that the change in stator blade surface roughness has little impact on the compressor performance. Thus, the leading factor of performance degradation is the increase in rotor blade surface roughness, which is consistent with the impact of roughness on the performance of single-stage compressors in the open literature [12–14,19].

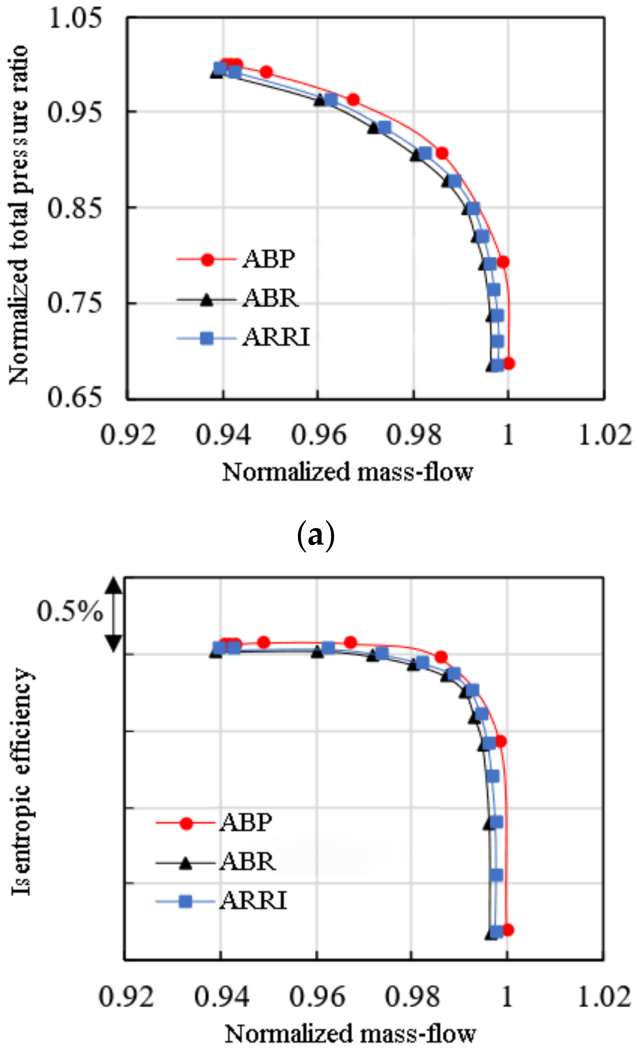

Figure 7. Comparison of compressor performance curves at design rotational speed under different roughness conditions. (**a**) Total pressure ratio versus mass flow, (**b**) Isentropic efficiency versus mass flow.

3.2. Influence of Roughness Variation on Compressor Stage Performance

According to the analysis in the previous subsection, increasing the blade surface roughness has little impact on the stable working range of the multistage compressor, but has a great impact on the peak total efficiency. This subsection discusses the stage where the roughness change has the greatest impact on the performance of the five-stage compressor at the design rotational speed.

Figure 8 gives the comparison of the distribution of entropy under the peak total efficiency condition when the blade surface roughness changes. By comparing the pitch-averaged flow field when all blades are roughened and polished, it can be seen that the entropy generation in the middle of the fifth stage blade is larger. It is preliminarily concluded that, when all of the blade surfaces become rough, the change in roughness has a relatively small impact on the performance of the front stage, and the change in roughness has a great impact on the performance of the fifth stage.

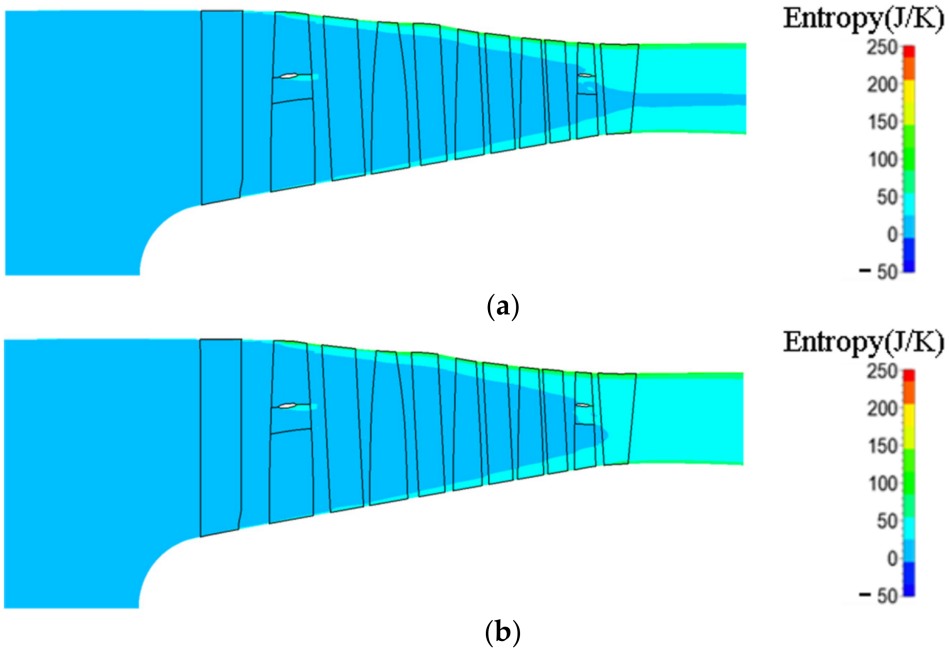

Figure 8. Comparison of pitch-averaged entropy distribution under the peak total efficiency with different roughness conditions. (**a**) ABPT, (**b**) ABRT.

In order to quantitatively analyze which stage performance is most sensitive to roughness change, a weight variable W_i is introduced. W_i is defined based on the definition of polytropic efficiency and can be used for any multi-stage axial compressor to evaluate the proportion of each stage efficiency decline in the total efficiency decline of the compressor. According to reference [29], the polytropic efficiency of the five-stage compressor η_P and the polytropic efficiency of each stage η_{Pi} can be depicted as:

$$\eta_p = \frac{\gamma - 1}{\gamma} \frac{\ln(P_5/P_0)}{\ln(T_5/T_0)} \tag{5}$$

$$\eta_{pi} = \frac{\gamma - 1}{\gamma} \frac{\ln(P_i/P_{i-1})}{\ln(T_i/T_{i-1})} \tag{6}$$

where γ is the isentropic coefficient of ideal gas; P_i and T_i represent the total pressure and the total temperature at position i, respectively; the subscript i represents the different axial positions as shown in Figure 1.

For the five-stage compressor studied, the total polytropic efficiency η_P can be written as:

$$\eta_p = \frac{\gamma - 1}{\gamma} \frac{1}{\ln(T_5/T_0)} \ln\left(\frac{P_5}{P_4} \times \frac{P_4}{P_3} \times \frac{P_3}{P_2} \times \frac{P_2}{P_1} \times \frac{P_1}{P_0}\right) = \frac{\gamma - 1}{\gamma} \frac{1}{\ln(T_5/T_0)} \sum_{i=1}^{5} \ln\left(\frac{P_i}{P_{i-1}}\right) \tag{7}$$

To obtain the relationship between the total polytropic efficiency and the stage polytropic efficiency, combing Equations (6) and (7) results in:

$$\eta_p = \frac{1}{\ln(T_5/T_0)} \sum_{i=1}^{5} \ln(T_i/T_{i-1}) \eta_{pi} \tag{8}$$

From Equation (8), the weight variable W_i can be extracted, which is defined as:

$$W_i = \frac{\ln(T_i/T_{i-1})}{\ln(T_5/T_0)} \; i = 1 \sim 5 \tag{9}$$

Therefore, the polytropic efficiency of the five-stage compressor can be weighted by the polytropic efficiency of each stage:

$$\eta_p = \sum_{i=1}^{5} W_i \eta_{pi} \tag{10}$$

Taking the total temperature ratio as the output work, from Equation (7), it is seen that the physical meaning of W_i is the ratio between the output work of each stage and the output work of the whole multistage axial compressor. Therefore, $\sum_{i=1}^{5} W_i = 1$. Because the ratio between the output work of each stage and the output work of the whole multistage axial compressor under peak total efficiency conditions is basically unchanged under different blade roughness, the quantitative analysis used in this paper was performed under the peak total efficiency condition. In such cases, the decrease in efficiency of each stage resulting from the blade roughness, $\Delta\eta_{pi}$, can be written as:

$$\Delta\eta_{pi} = W_i\left(\eta_{pi}|_{roughness} - \eta_{pi}|_{smooth}\right) \; i = 1 \sim 5 \tag{11}$$

where $\eta_{pi}|_{smooth}$ is the stage polytropic efficiency after polishing all blades and $\eta_{pi}|_{roughness}$ is the stage polytropic efficiency when all blades are rough.

The histogram of the weight variable value and efficiency decline value of each compressor stage is given in Figure 9. It can be seen that the quantitative analysis clearly quantifies the influence of blade surface roughness at all stages on the performance of the whole compressor. Specifically, the weight variable values of the first stage and the second stage are higher than those of the latter three stages. However, from the degree of efficiency decline, it can be observed that the latter three stages contribute the most to the efficiency decline of the whole compressor, especially the fifth stage, with the largest proportion of efficiency decline of up to 0.32%.

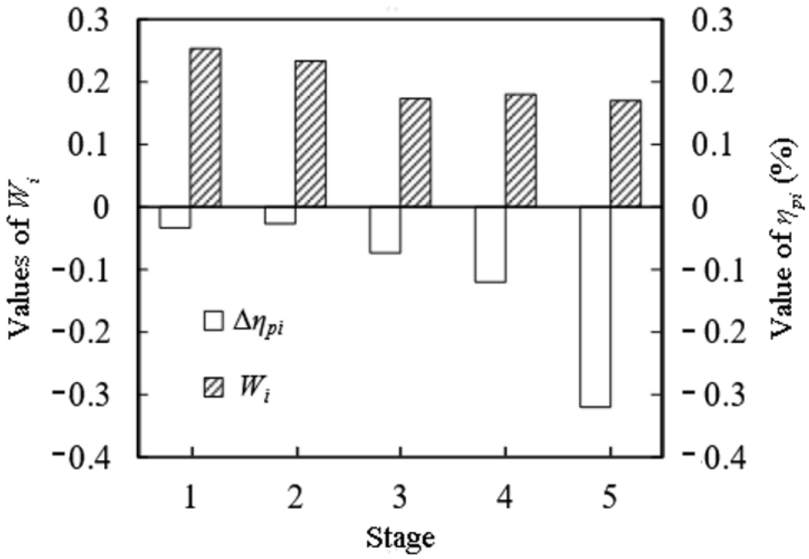

Figure 9. Histogram of weight variable value and efficiency decline value of each compressor stage.

Combined with the above qualitative and quantitative analysis results of the flow field, when all blades become rough, the performance of the later stage is more sensitive to the change in roughness than that of the previous stage, and the decline in the performance of the fifth stage contributes the most to the decline in the overall performance.

In order to explore the mechanism of the change in blade surface roughness affecting the overall performance, a flow detail analysis is carried out below. Since the decline in the fifth stage performance contributes the most to the decline in the overall performance, the flow field of the fifth stage is mainly analyzed here. Figure 10 shows the entropy

generation distribution along the span of the fifth stage at the inlet and outlet for different roughness conditions under the peak total efficiency condition. The red curve represents the entropy distribution of the fifth stage with all rough blades, and the blue curve refers to the entropy distribution of the fifth stage with all polished blades. When the span is determined, the difference between the entropy at the outlet and inlet of the fifth stage is the entropy generation of the fifth stage at the span. It indicates that, in the region below a 20% span, the entropy generation in the blade rough state is smaller than that in the polishing state, indicating that the flow loss near the fifth stage root is smaller after the blade surface becomes rough. Moreover, in the range of a 30% to 70% span, the entropy generation in the blade rough state is significantly larger than that in the polishing state, which reveals that the flow loss near the middle of the fifth stage increases significantly after the blade surface becomes rough.

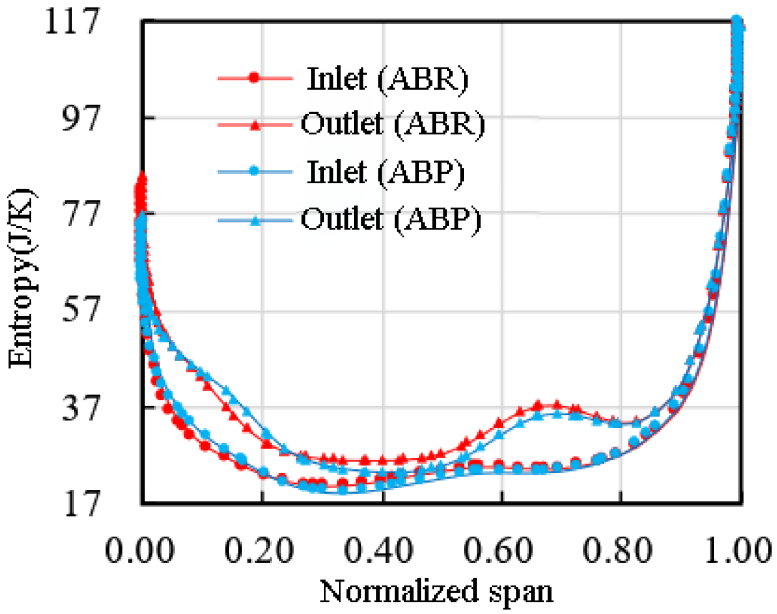

Figure 10. The entropy distribution along span at the inlet and outlet of the fifth stage under peak total efficiency conditions.

The limit streamlines of the suction surface of the fifth stage for different roughness conditions under the peak total efficiency condition are displayed in Figure 11. Among them, the red limit streamlines donate the boundary layer separation lines on the surface. The limit streamlines on the rotor suction surface imply that, in the polishing state, the separation line extends from the blade root to the vicinity of the middle of the blade, then reattaches and extends to the lower end of the damper. However, once the blade surface becomes rough, the axial length of the recirculation zone caused by the separation near the blade root decreases, and the separation line extends from the blade root to the lower end of the damper without disconnection in the middle of the blade. Therefore, the recirculation zone near the middle of the blade is slightly larger than that in the polished state. From the change in the limit streamline on the rotor suction surface, it is seen that, as the blade surface roughness increases, the recirculation zone at the blade root of the stator suction surface decreases significantly, and the spanwise height of the recirculation zone decreases from the original 30% span to a 20% span.

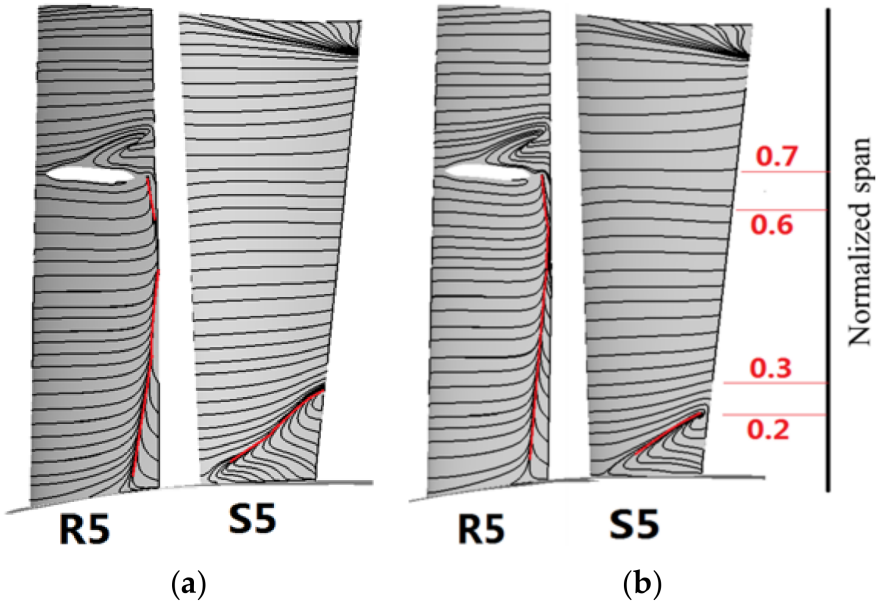

Figure 11. The limit streamline distribution of blade suction surface of the fifth stage under peak total efficiency conditions. (**a**) ABP, (**b**) ABR.

According to the analysis results in Figures 10 and 11, it can be concluded, after all blades become rough, the boundary layer separation phenomenon near the root of the rotor and stator in the fifth stage will be improved and the aerodynamic loss in the corresponding region will be reduced. However, it will increase the separation near the middle of the rotor in the fifth stage increase and increase the corresponding aerodynamic loss. As known from the analysis of Figure 6, the fifth stage is the stage with the largest reduction in stage efficiency after all blades are roughened. Therefore, the main reason for the decline in the overall performance can be attributed to the deterioration of separation flows near the middle of the rotor in the fifth stage.

3.3. Influence of Roughness Variation in the Fifth Stage on Compressor Performance

According to the analysis in Section 3.2, it is inferred that the main reason for the decline in the overall performance of the five-stage compressor is the increment of the roughness of the fifth-stage rotor. For the purpose of further verifying this inference, a numerical simulation and analysis of the influence of the individual change in the surface roughness for the rotor in the fifth stage at the design rotational speed were carried out in the following.

Figure 12 compares the flow efficiency characteristics of the compressor when the fifth stage rotor is roughened alone and when all blades are polished. The mass flow in the figure is normalized by the experimentally measured blocking flow. Moreover, the red and blue curves represent the flow efficiency characteristic curves of ABP and R5 roughened individually (R5RI), respectively. It can be seen from the zoomed-in view that, when the rotors of the fifth stage are roughened, the peak total efficiency of the compressor decreases compared with when all blades are polished.

Table 3 shows the decrease in and proportion of peak total efficiency for different blade roughness conditions. The decrease represents the relative drop of the peak total efficiency in the case of blade roughness compared with that in the case of all blades polished. The decrease proportion represents the ratio of the decrease in the case of blade roughness to the decreased amount in the case of all blades polished. It can be observed that, when all blades are roughened, the peak total efficiency of the compressor decreases by approximately 0.67%. When all rotor blades are roughened, the peak total efficiency of the compressor decreases by approximately 0.44%, and the decrease proportion is 65.7%. These phenomena further indicate that the increase in rotor blade surface roughness is the leading factor

for the decline in the overall efficiency, which is consistent with the conclusion obtained by the analysis of Figure 3. In addition, when the rotors in the fifth stage are roughened individually, the peak total efficiency of the compressor decreases by approximately 0.27%, and the decrease proportion is 65.7%. This further demonstrates that the increase in the blade surface roughness in the fifth stage has the greatest impact on the performance of the multistage compressor.

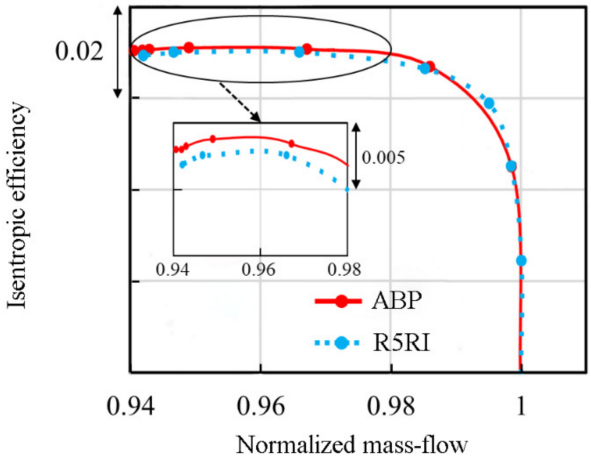

Figure 12. Comparison of compressor flow efficiency characteristics under different roughness conditions.

Table 3. The decreased amount and proportion of peak total efficiency of the compressor under different roughness conditions.

Roughness Condition	Decrease Amount	Decrease Proportion
ABR	0.67%	100%
ARRI	0.44%	65.7%
R5RI	0.27%	40.3%

Figure 13 displays the rotor efficiency and stage efficiency versus stage under peak total efficiency conditions when all blades are roughened and when the rotors in the fifth stage are roughened individually. It is depicted that, when the rotor blade in the fifth stage becomes rough, the rotor efficiency and stage efficiency of the fifth stage decrease, whereas the rotor efficiency and stage efficiency of other stages are almost unchanged. Therefore, it can be concluded that the increase in the surface roughness of rotor blades in the fifth stage has little impact on the performance of other stages, and mainly has a negative effect on the performance of the stage, which reduces the overall performance of the five-stage compressor.

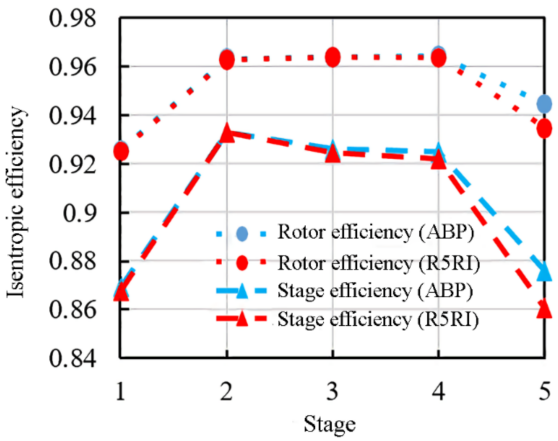

Figure 13. Rotor efficiency and stage efficiency versus stage under peak efficiency condition.

Figure 14 shows the limit streamline of the suction surface of the fifth stage blade for different roughness under the peak efficiency condition. ABP and ABR have been compared earlier, and this comparison will not be repeated here. From Figure 14b,c it is seen that, when the rotors in the fifth stage are roughened individually, the near-wall flow characteristics of the rotor and stator in the fifth stage are similar to those when all blades are roughened; that is, the recirculation zone near the middle of the rotor expands and the recirculation zone near the blade root of the stator decreases.

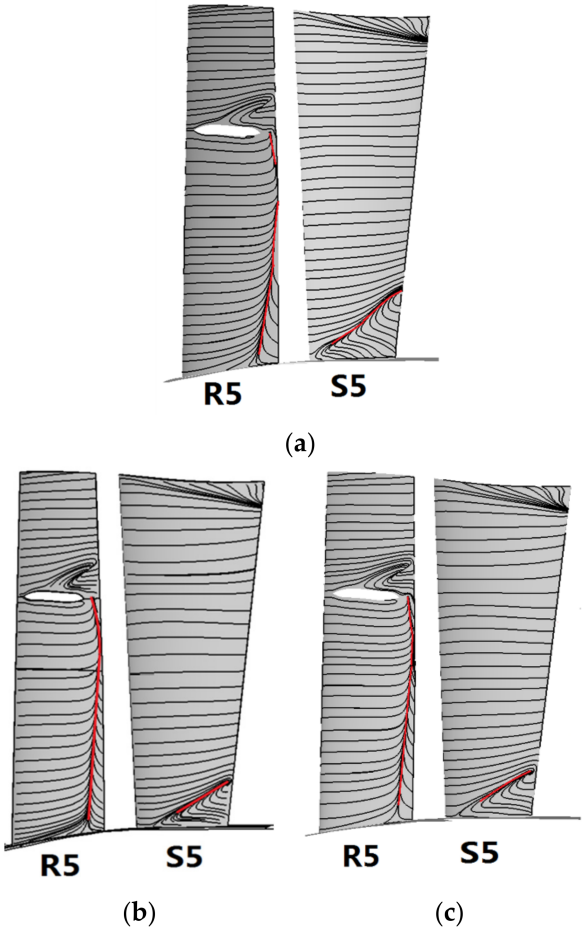

Figure 14. Limit streamline distribution of blade suction surface of fifth stage under peak efficiency conditions. (**a**) ABP, (**b**) R5RI, (**c**) ABR.

To sum up, with the increase in the surface roughness of the fifth stage blade, the flow in the middle of the rotors in the fifth stage deteriorates and the stage performance decreases significantly, resulting in a decline in the overall performance. This means that the increase in the surface roughness for the fifth stage rotor is the main reason for the decline in the overall performance.

4. Conclusions

Based on the real measured blade surface roughness data, this paper used the equivalent gravel roughness model to model the blade surface roughness. Then, using the full three-dimensional numerical simulation method, the impact of blade surface roughness on the performance change in the five-stage compressor of an engine in service at design rotational speed was analyzed. Finally, combined with quantitative analysis and flow field analysis, the mechanism of the performance degradation caused by roughness was revealed. The main conclusions are as follows:

(1) When the surface roughness of all blades increases, the blocking mass flow, peak total efficiency, and peak total pressure ratio decrease, while the stable working range

changes little. When only the rotor surfaces become rough, the performance degradation range is close to that of all rotor and stator blades roughened. Therefore, the change in the roughness of the stators has little impact on the overall performance of the compressor.

(2) When all rotors and stators are roughened, the performance of the rear stage is more sensitive to the change in roughness than that of the front stage, and the decline in the performance of the fifth stage contributes the most to the decline in the overall performance. Meanwhile, the recirculation zone near the blade root of the rotors and stators in the fifth stage decreases, and the aerodynamic loss in the corresponding region decreases. However, the recirculation zone near the middle span of the rotors in the fifth stage expands, and the corresponding aerodynamic loss increases.

(3) The increase in the surface roughness of the rotors in the fifth stage imposes a negative effect on the performance of the stage itself but shows a marginal influence on the performance of other stages. With the increase in surface roughness for the blades in the fifth stage, the flows in the middle span of the rotors in the fifth stage deteriorate, and the stage performance decreases significantly, resulting in a decline in the overall performance of the compressor.

Author Contributions: Conceptualization, Y.C.; methodology, Y.C. and W.C.; software, Y.C. and C.G.; validation, Y.C.; formal analysis, Y.C. and C.G.; investigation, Y.C. and C.G.; writing—original draft preparation, Y.C., C.G. and W.C.; writing—review and editing, Y.C., C.G. and W.C.; supervision, Y.C. and W.C. All authors have read and agreed to the published version of the manuscript.

Funding: This research supported by the National Natural Science Foundation of China (Grant No.51576162) and national key scientific and technological project of China (Grant No.2017-II-0005-0018).

Institutional Review Board Statement: Not applicable.

Informed Consent Statement: Not applicable.

Data Availability Statement: Not applicable.

Acknowledgments: Special thanks are addressed to the Laboratory of Rotating Flow and Heat Transfer at Northwestern Polytechnical University.

Conflicts of Interest: The authors declare no conflict of interest.

References

1. Diakunchak, I.S. Performance Deterioration in Industrial Gas Turbines. *J. Eng. Gas Turbines Power* **1992**, *114*, 161–168. [CrossRef]
2. Yuan, J.; Piomelli, U. Roughness Effects on the Reynolds Stress Budgets in Near-Wall Turbulence. *J. Fluid Mech.* **2014**, *760*, R1. [CrossRef]
3. Yang, X.; Meneveau, C. Large Eddy Simulations and Parameterisation of Roughness Element Orientation and Flow Direction Effects in Rough Wall Boundary Layers. *J. Turbul.* **2016**, *17*, 1072–1085. [CrossRef]
4. Smits, A.J.; Mckeon, B.J.; Marusic, I. High–Reynolds Number Wall Turbulence. *Annu. Rev. Fluid Mech.* **2011**, *43*, 353–375. [CrossRef]
5. Gao, W.; Zhang, W.; Cheng, W.; Samtaney, R. Wall-Modelled Large-Eddy Simulation of Turbulent Flow Past Airfoils. *J. Fluid Mech.* **2019**, *873*, 174–210. [CrossRef]
6. De Vanna, F.; Cogo, M.; Bernardini, M.; Picano, F.; Benini, E. Unified Wall-Resolved and Wall-Modeled Method for Large-Eddy Simulations of Compressible Wall-Bounded Flows. *Phys. Rev. Fluids* **2021**, *6*, 034614. [CrossRef]
7. Bernardini, M.; Pirozzoli, S.; Orlandi, P. Compressibility Effects on Roughness-Induced Boundary Layer Transition. *Int. J. Heat Fluid Flow* **2012**, *35*, 45–51. [CrossRef]
8. Redford, J.A.; Sandham, N.D.; Roberts, G.T. Compressibility Effects on Boundary-Layer Transition Induced by an Isolated Roughness Element. *AIAA J.* **2010**, *48*, 2818–2830. [CrossRef]
9. Bammert, K.; Milsch, R. *Boundary Layers on Rough Compressor Blades*; ASME Paper GT1972-48; American Society of Mechanical Engineers: New York, NY, USA, 1972.
10. Back, S.C.; Hobson, G.V.; Song, S.J.; Millsaps, K.T. Effects of Reynolds Number and Surface Roughness Magnitude and Location on Compressor Cascade Performance. *J. Turbomach.* **2012**, *134*, 051013. [CrossRef]
11. Suder, K.L.; Chima, R.V.; Strazisar, A.J.; Roberts, W.B. The Effect of Adding Roughness and Thickness to a Transonic Axial Compressor Rotor. *J. Turbomach.* **1995**, *117*, 491–505. [CrossRef]
12. Morini, M.; Pinelli, M.; Spina, P.R.; Venturini, M. Numerical Analysis of the Effects of Nonuniform Surface Roughness on Compressor Stage Performance. *J. Eng. Gas Turbines Power* **2011**, *133*, 125–132. [CrossRef]
13. Aldi, N.; Morini, M.; Pinelli, M.; Spina, P.R.; Suman, A.; Venturini, M. Numerical Analysis of the Effects of Surface Roughness Localization on the Performance of an Axial Compressor Stage. *Energy Procedia* **2014**, *45*, 1057–1066. [CrossRef]

14. Aldi, N.; Morini, M.; Pinelli, M.; Spina, P.R.; Suman, A.; Venturini, M. Performance Evaluation of Non-Uniformly Fouled Axial Compressor Stages by Means of Computational Fluid Dynamic Analyses. *J. Turbomach.* **2014**, *136*, 021016. [CrossRef]
15. Gao, L.; Wang, Z.; Geng, S.; Zhang, H.; Nie, C. Experimental Study for Effects of Surface Roughness on Compressor Cascade Loss Characteristics. *J. Propuls. Technol.* **2016**, *37*, 1263–1270. (In Chinese)
16. Liu, K.; Chu, W.; Zhang, H.; Chen, X.; Li, J.; Li, L. Effectiveness of Blade Surface Roughness on 3D Corner Separation and Loss in Compressor Cascades. *J. Propuls. Technol.* **2019**, *40*, 504–514. (In Chinese)
17. Wang, M.; Li, Z.; Lu, X.; Zhao, S.; Zhang, Y. The Control Mechanism for the Boundary Layer of a High Subsonic Compressor Airfoil by Surface Roughness Under Different Reynolds Numbers. *J. Eng. Thermophys.* **2019**, *40*, 504–514. (In Chinese)
18. Chen, S.; Chen, Z.; Hui, S.; Wang, S.; Wang, Z. *Study on the Impact of Fouling on Axial Compressor Stage*; ASME Paper GT2012-68041; American Society of Mechanical Engineers: New York, NY, USA, 2012.
19. Benini, E. Three-Dimensional Multi-Objective Design Optimization of a Transonic Compressor Rotor. *J. Propuls. Power* **2004**, *20*, 559–565. [CrossRef]
20. Pinto, R.N.; Afzal, A.; D' Souza, L.V.; Ansari, Z.; Mohammed Samee, A.D. Computational Fluid Dynamics in Turbomachinery: A Review of State of the Art. *Arch. Comput. Methods Eng.* **2017**, *24*, 467–479. [CrossRef]
21. Li, Z.; Zheng, X. Review of Design Optimization Methods for Turbomachinery Aerodynamics. *Prog. Aerosp. Sci.* **2017**, *93*, 1–23. [CrossRef]
22. Braembussche, R.A. Numerical Optimization for Advanced Turbomachinery Design. In *Optimization and Computational Fluid Dynamics*; Springer: Berlin/Heidelberg, Germany, 2008; pp. 147–189.
23. De Vanna, F.; Bof, D.; Benini, E. Multi-Objective RANS Aerodynamic Optimization of a Hypersonic Intake Ramp at Mach 5. *Energies* **2022**, *15*, 2811. [CrossRef]
24. Chen, Y.; Lin, A.; Zhang, H.; Chu, W. Method of Improving Stability of a Highly-Loaded Axial Compressor Stage by Coupling Different Casing Treatments. *J. Appl. Fluid Mech.* **2022**, *15*, 645–657.
25. Schlichting, H. Experimental Investigation of the Problem of Surface Roughness. *Tech. Rep. Arch. Image Libr.* **1936**, *7*, 747–748.
26. Goodhand, M.N.; Walton, K.; Blunt, L.; Lung, H.W.; Miller, R.J.; Marsden, R. *The Limitations of "Ra" to Describe Surface Roughness*; ASME Paper GT2015-43329; American Society of Mechanical Engineers: New York, NY, USA, 2015.
27. Bons, J.P. A Review of Surface Roughness Effects in Gas Turbines. *J. Turbomach.* **2010**, *132*, 021004. [CrossRef]
28. White, F.M. *Viscous Fluid Flow*; McGraw-Hill: New York, NY, USA, 1991.
29. Qi, D. *Principle of Centrifugal Compressor*; China Machine Press: Beijing, China, 2019. (In Chinese)